Society for
Mathematical
Biology

ORIGINAL ARTICLE

Optimal Control with RdCVFL for Degenerating Photoreceptors

Kathryn Wifvat[1] · Erika T. Camacho[1,2,4,5,6] · Matthias Kawski[1] ·
Thierry Léveillard[4,5,6] · Stephen Wirkus[2,3]

Abstract

Both the rod and cone photoreceptors, along with the retinal pigment epithelium have been experimentally and mathematically shown to work interdependently to maintain vision. Further, the theoredoxin-like rod-derived cone viability factor (RdCVF) and its long form (RdCVFL) have proven to increase photoreceptor survival in experimental results. Aerobic glycolysis is the primary source of energy production for photoreceptors and RdCVF accelerates the intake of glucose into the cones. RdCVFL helps mitigate the negative effects of reactive oxidative species and has shown promise in slowing the death of cones in mouse studies. However, this potential treatment and its effects have never been studied in mathematical models. In this work, we examine an optimal control with the treatment of RdCVFL. We mathematically illustrate the potential this treatment might have for treating degenerative retinal diseases such as retinitis pigmentosa, as well as compare this to the results of an updated control model with RdCVF.

✉ Stephen Wirkus
    stephen.wirkus@utsa.edu

1   School of Mathematical and Statistical Sciences, Arizona State University, Tempe, AZ 85287,
    USA

2   Department of Mathematics, The University of Texas at San Antonio, San Antonio, TX 78249,
    USA

3   School of Mathematical and Natural Sciences, Arizona State University, Glendale, AZ 85306,
    USA

4   INSERM, U968, 75012 Paris, France

5   UPMC Univ Paris 06, UMR_S 968, Institut de la Vision, Sorbonne Universités, 75012 Paris,
    France

6   CNRS, UMR_7210, 75012 Paris, France

1 Introduction

1.1 Background of Retinitis Pigmentosa and RdCVFL

Vision impairment is a serious problem that affects at least 2.2 billion people worldwide. Cataracts and glaucoma are the two most common causes of blindness in the world because developing countries rarely have access to the medical treatments needed to stop their progression and vision damage (Steinmetz et al. 2021). In contrast, the biggest contributors to vision loss in developed countries with no cure are due to photoreceptor degeneration, such as in age-related macular degeneration (AMD), untreated retinal detachment, and retinitis pigmentosa (RP) (Steinmetz et al. 2021). While a lot is known about these maladies, they still remain uncurable. The leading cause of inherited retinal degeneration that can cause complete loss of vision is RP, which affects about 1 in 4000 people (Besharse and Bok 2011; Shintani et al. 2009). RP is a heterogenous group of diseases characterized by rod photoreceptor death due to one of many different genetic mutations in the rods followed by the death of otherwise healthy cones. The evolving belief among experimentalists is that a combination of starvation and hyperoxia lead to this secondary cone death (Kanan et al. 2022; Léveillard and Sahel 2017; Petit et al. 2018). Recent experimental work has shown that the rod-derived cone viability factor (RdCVF), which is exclusively produced by the rods, increases glucose uptake by the cones; its long form (RdCVFL), produced by both rods and cones, has been shown to reduce photoreceptor degeneration by protecting against oxidative stress (Aït-Ali et al. 2015; Byrne et al. 2015; Elachouri et al. 2015; Léveillard et al. 2004). Thus, RdCVF and RdCVFL together provide a concrete link between starvation and hyperoxia once the rods have degenerated (Byrne et al. 2015; Elachouri et al. 2015; Léveillard and Sahel 2017). Mathematical work has confirmed the respective roles of RdCVF and RdCVFL as well (Aparicio et al. 2022; Camacho and Wirkus 2013; Camacho et al. 2014, 2016, ?, 2019, 2021; Dobreva et al. 2022; Wifvat et al. 2021).

Both RdCVF and RdCVFL are encoded in the cDNA Nucleoredoxin-like (*Nxnl1*) gene (Chalmel et al. 2007; Léveillard et al. 2004). RdCVFL is a member of the thioredoxin family and includes a C-terminal extension that confers enzymatic activities (Brennan et al. 2010; Funato and Miki 2007) whereas RdCVF is truncated and has no enzymatic activity (Chalmel et al. 2007). However RdCVF is necessary to stabilize GLUT1 in the plasma membrane of photoreceptors, by binding to basigin-1 (Bsg1), in order to enhance glucose uptake (Aït-Ali et al. 2015). Thioredoxin is an important regulator of cellular redox homeostasis, which catalyzes the reduction of disulfide bonds and in humans it has been implicated in a wide variety of intracellular and extracellular redox regulations (Matsuo and Kimura-Yoshida 2013).

The rods produce the thioredoxin enzymatic protein RdCVFL as well as the trophic factor RdCVF through a process called alternative splicing. Cones on the other hand, only produce RdCVFL (Aït-Ali et al. 2015; Byrne et al. 2015). Therefore, both cones and rods express the RdCVFL protein and it is also helpful to both types of photoreceptor in protecting them from photo-oxidative damage (such as the oxidation of polyunsaturated fatty acids). In mice studies, it has been shown that RdCVFL reduces

the effects of photoreceptor degeneration (Byrne et al. 2015). Just like any other protein from the thioredoxin family, the thiol oxidoreductase activity of RdCVFL depends on how high or reduced its oxidized status is. The thioredoxin reductases step in to reduce RdCVFL whenever it becomes oxidized (Léveillard et al. 2017). Usually produced from glucose in the pentose phosphate pathway, nicotinamide adenine dinucleotide phosphate (NADPH) is the cofactor of these reductases and thus most likely RdCVF provides a reducing power to RdCVFL (Dobreva et al. 2023; Léveillard et al. 2017). With a retinal disease such as RP, if the rods die then RdCVF is lost, which contributes to the secondary wave of cone death. It is speculated that part of the reason for the secondary cone death could be a result of oxidative damage due to the loss of RdCVFL from the rods (Elachouri et al. 2015) and thus it is necessary to study both RdCVF and RdCVFL to enhance our understanding of possible therapies that may prevent secondary cone deaths. However the first step towards investigating the joint effect of RdCVFL and RdCVF is to investigate the effects of each separately.

According to Mei et al. (2016), RdCVF is secreted by rods and protects cones by stimulating aerobic glycolysis when it interacts with glucose transporter 1 (GLUT1) and a complex containing basigin-1. The role of *Nxnl1* is studied in cones in this paper. Because RdCVFL is encoded by the *Nxnl1* gene, we consider *Nxnl1* to be a proxy for RdCVFL and thus the absence of RdCVFL is represented by the *Nxnl1-/-* mouse (a "knockout" mouse created to *not* have the *Nxnl1* gene (Elachouri et al. 2015)). The studies with mice confirm that damage produced by oxidative stress in cones can be reduced through the administration of RdCVFL to mice that have the genetic abnormality of a deletion of the *Nxnl1* gene (Elachouri et al. 2015). Further, RdCVFL is also shown to have cell-autonomous protection since cell viability is reduced when the RdCVFL expression is silenced in a cone-enriched culture (Elachouri et al. 2015). Thus both RdCVF and RdCVFL protect the cones in different ways and are each important and can both be incorporated into a treatment or therapy for RP.

RdCVFL protects rod and cone photoreceptors against photo-oxidative stress and damage as shown in mice studies (Byrne et al. 2015; Elachouri et al. 2015). The *rd10* mice are models of RP (e.g., see Phillips et al. 2010) and it is shown that RdCVFL reduces the oxidation of polyunsaturated fatty acids caused by the degeneration of photoreceptors (Byrne et al. 2015). Since RdCVFL includes a thioredoxin fold and RdCVF does not (however, it contains the thioredoxic catalytic site sequence CXXC), RdCVF has no thiol oxidoreductase activity (Léveillard et al. 2017). It is shown in Mei et al. (2016) that cones protect themselves against oxidative stress during aging as they produce RdCVFL. It has further been shown in mouse studies (Elachouri et al. 2015) and previous mathematical work (Wifvat et al. 2021) that RdCVFL can slow the death of cones by mitigating the negative effects of reactive oxidative species (ROS) (Clérin et al. 2011). Knowing how RdCVF and RdCVFL both interact with the cones sheds light on RP and suggests the potential for a double-therapeutic approach involving administration of both RdCVF and RdCVFL. Since potential theraputic effects of RdCVF have been studied previously, in this work, we will study the individual treatment with RdCVFL.

It has been experimentally shown previously by Mei et al. (2016), that RdCVFL causes a rescue effect for the cones. It has also been shown that RdCVFL is not expressed in the retinal pigment epithelium (RPE) of the *rd1* mouse (Mei et al. 2016;

Léveillard and Sahel 2017, another mouse model of RP) but it is expressed in the photoreceptors of the eye. In lab studies with mice and a control group, RdCVFL was shown to reduce the damage done to cones by as much as 63% (Elachouri et al. 2015). The RdCVFL was subretinally injected after rods had degenerated and then the cone function was recorded. It was found that RdCVFL was able to protect cones from the secondary wave of death after rods had died by as much as 47% (Elachouri et al. 2015). One hypothesis of how this works is that after the rods die off and thus RdCVF is no longer being expressed, there is then less RdCVFL and a higher amount of oxidative stress which causes the cones to die (Léveillard and Sahel 2010). Thus, this protein shows a lot of promise for protecting cones even after rods have died, such as in later stages of RP.

A previous mathematical model looked at the administration of RdCVF and used optimal control theory to obtain the same rescue effect that was observed experimentally (Camacho et al. 2014). To the knowledge of the authors, this was the first use of optimal control utilizing treatment to try to prevent photoreceptor degeneration; a subsequent paper incorporating a different treatment via mesencephalic astrocyte-derived neurotrophic factor (MANF) again incorporated optimal control to reproduce the observed experimental data (Camacho et al. 2020). Optimal control has been used in a wide range of applications in mechanical engineering, economics, and a range of other disciplines (see, e.g., Athans and Falb 2013; Bryson 1975; Kirk 2004; Pontryagin 1987). In recent decades, optimal control in biological applications has become increasingly utilized (Lenhart and Workman 2007). Some applications to biological problems have included drug administration in chemotherapy, treatment strategies in epidemics, and population harvesting models to name a few (see, e.g., Lenhart and Workman (2007)).

This will be the first mathematical model of photoreceptors that includes optimal control treatment with RdCVFL to counteract photoreceptor degeneration. This information can potentially be used for developing treatments for trials. With optimal control, we maximize the amount of photoreceptors while minimizing the toxicity due to the potential treatments, to find the optimal amount of potential treatment for maintaining vision. Specifically, it is important to understand how the presence of RdCVFL impacts the cones and rods so that if a patient has a disease that affects their vision, potential treatments including RdCVFL can be used to help the patient maintain their night or peripheral vision as well as their central vision.

2 ODE Model with RdCVFL Control and Derivations

The results presented in this manuscript build from the system of equations modeling the ecosystem of the rod cells, cone cells, and retinal pigmented epithelium (RPE):

$$\frac{dR_n}{dt} = \underbrace{aR_nT}_{\substack{\text{renewal}\\\text{associated}\\\text{metabolism}}} - \underbrace{\mu_n}_{\substack{\text{shedding}\\\text{associated}\\\text{metabolism}}} \cdot \underbrace{\left(\frac{R_n}{B_1 + \delta_r R_n}\right)}_{\substack{\text{RdCVFL protection}\\\text{against oxidative stress}}} \tag{1}$$

Table 1 Parameter descriptions and units; also, see Wifvat et al. (2021)

Parameter	Description	Units
a_n	Renewal and assoc. metabolism of rod OS mediated by T	$\frac{1}{\text{day mM}}$
β_n	Removal rate of nutrients from T by R	$\frac{1}{\text{day (rod OS)}}$
γ	Removal rate of nutrients from T by C	$\frac{1}{\text{day (cone OS)}}$
Γ	Total inflow rate into the T	$\frac{1}{\text{day}}$
κ	Limiting capacity of trophic factors	$\frac{1}{\text{day mM}}$
μ_n	Metabolism assoc. w. energy cons & shedding of R	$\frac{\text{mM}}{\text{day}}$
μ_c	Metabolism assoc. w. energy cons & shedding of C	$\frac{\text{mM}}{\text{day}}$
K_{mg}	Substrate concentration that gives half $V_{\max}$	mM
B_1	Quantification of reactive oxygen species for R	mM
B_2	Quantification of reactive oxygen species for C	mM
$V_{\max}$	Limiting value of the transport rate of glucose	$\frac{\text{mM}}{\text{day}}$
δ_n	Per cell conc. of RdCVF synthesized by R	$\frac{\text{mM}}{\text{rod OS}}$
δ_r	Per cell conc. of RdCVFL expressed by R helps R	$\frac{\text{mM}}{\text{rod OS}}$
δ_c	Per cell conc. of RdCVFL expressed by C helps C	$\frac{\text{mM}}{\text{cone OS}}$
ν_2	Conversion factor	$\frac{1}{\text{mM}^2}$
p	Rate of glucose uptake in C in absence of RdCVF	$\frac{\text{mM}}{\text{day}}$

The RdCVFL parameters, δ_c and δ_r, are nonnegative; all other parameters are positive

$$\frac{dC}{dt} = \nu_2 \underbrace{\left(\frac{V_{\max}(\delta_n R_n)^2}{K_{mg}^2 + (\delta_n R_n)^2} + p \right) CT}_{\substack{\text{renewal associated metabolism, including} \\ \text{increase in glucose uptake due to RdCVF}}} - \underbrace{\mu_c}_{\substack{\text{shedding} \\ \text{associated} \\ \text{metabolism}}} \cdot \underbrace{\left(\frac{C}{B_2 + \delta_c C} \right)}_{\substack{\text{RdCVFL protection} \\ \text{against oxidative stress}}} \qquad (2)$$

$$\frac{dT}{dt} = \underbrace{T(\Gamma - \kappa T)}_{\substack{\text{carrying capacity of} \\ \text{nutrient pool \& glucose,} \\ \text{mediated by the RPE}}} - \underbrace{T(\beta_n R_n + \gamma C)}_{\substack{\text{net removal of nutrients} \\ \text{\& glucose from trophic} \\ \text{pool by photoreceptors}}} \qquad (3)$$

which was analyzed in Wifvat et al. (2021); R_n is the cumulative proportion of full length rod outer segments (OS), C is the cumulative proportion of full length cone outer segments, and T is the nutrients, including glucose, and other trophic factors mediated by the RPE. The parameters and their meanings are listed in Table 1 (Wifvat et al. 2021).

We now introduce a control function to the model (1)–(3) to study the effects that RdCVFL treatment has on its equilibrium solutions. The system of equations modified to include the control $u \in [0, 1]$ has effectiveness of treatment parameters σ_1 and σ_2 where the value for σ_1 is 192, which is $\delta_r R_{n0}$ rounded to the nearest whole number, and σ_2 is 234, $\delta_c C_0$ rounded to the nearest whole number where $R_n 0$ and C_0 are the

initial cumulative portion of full length of rod and cone outer segments, respectively.

$$\frac{dR_n}{dt} = R_n T a_n - \mu_n \left(\frac{R_n}{B_1 + u\sigma_1} \right) \tag{4}$$

$$\frac{dC}{dt} = \nu_2 \left(\frac{V_{\max}(\delta_n R_n)^2}{K_{mg}^2 + (\delta_n R_n)^2} + p \right) CT - \mu_c \left(\frac{C}{B_2 + u\sigma_2} \right) \tag{5}$$

$$\frac{dT}{dt} = T(\Gamma - \kappa T - \beta_n R_n - \gamma C). \tag{6}$$

This system can be defined as the following for the rest of the paper,

$$\dot{x} = f(x, u), \tag{7}$$

for convenience, with $x = (R_n, C, T)$. The treatment that administers RdCVFL is incorporated into the system in the second term of (4) and (5) as u, the control function of time t. This treatment is in the form of a subretinal injection of an adeno-associated virus (AAV) vector. Upon the injection of the AAV, the pumping mechanisms of the RPE cause the gradual and complete absorption of the fluid (Martin et al. 2002).

Standard methods in optimal control do not apply due to the nonlinear manner in which the control appears in the system. We thus linearize the system in order to show existence of a control for the linear system and then compare with the nonlinear results. Here the variables and parameters R_n, C, B_1 and B_2 are rearranged, only in the terms that include the control u, to set up the equations to be linearized in the next step:

$$\frac{dR_n}{dt} = R_n T a_n - \mu_n \frac{R_n}{B_1} \left(\frac{1}{1 + \frac{\sigma_1}{B_1} u} \right) \tag{8}$$

$$\frac{dC}{dt} = \nu_2 \left(\frac{V_{\max}(\delta_n R_n)^2}{K_{mg}^2 + (\delta_n R_n)^2} + p \right) CT - \mu_c \frac{C}{B_2} \left(\frac{1}{1 + \frac{\sigma_2}{B_2} u} \right) \tag{9}$$

$$\frac{dT}{dt} = T(\Gamma - \kappa T - \beta_n R_n - \gamma C). \tag{10}$$

The linearization (first order Taylor's approximation about $u = 0$) is

$$\frac{dR_n}{dt} = R_n T a_n - \mu_n \frac{R_n}{B_1} \left(1 - \frac{\sigma_1}{B_1} u \right) \tag{11}$$

$$\frac{dC}{dt} = \nu_2 \left(\frac{V_{\max}(\delta_n R_n)^2}{K_{mg}^2 + (\delta_n R_n)^2} + p \right) CT - \mu_c \frac{C}{B_2} \left(1 - \frac{\sigma_2}{B_2} u \right) \tag{12}$$

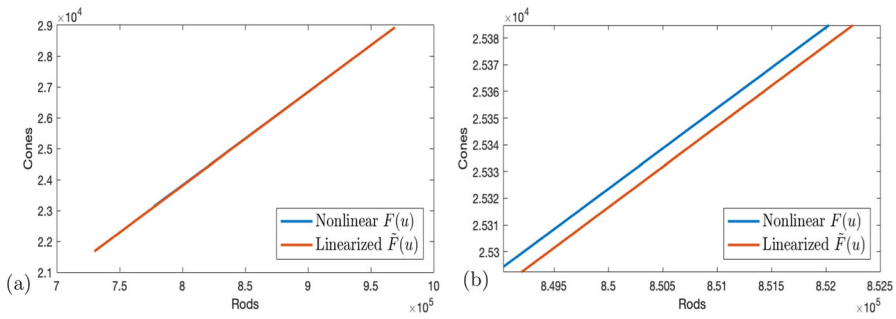$$\frac{dT}{dt} = T(\Gamma - \kappa T - \beta_n R_n - \gamma C). \tag{13}$$

Fig. 1 (Color figure online) **a** Left panel: the plots of $F(u)$ and $\tilde{F}(u)$. Observe that these are practically indistinguishable at this scale. Right panel: Zoomed in plots of $F(u)$ and $\tilde{F}(u)$

This system can be defined as the following for the rest of the paper:

$$\dot{x} = f_l(x, u), \tag{14}$$

for convenience, with $x = (R_n, C, T)$.

Further, we will compare the control terms of the nonlinear (4)–(6) and linearized (11)–(13) models:

$$F(u) = \begin{cases} \mu_n \left(\dfrac{R_n}{B_1 + u\sigma_1} \right) \\ \mu_c \left(\dfrac{C}{B_2 + u\sigma_2} \right) \end{cases} \tag{15}$$

$$\tilde{F}(u) = \begin{cases} \mu_n \dfrac{R_n}{B_1} \left(1 - \dfrac{\sigma_1}{B_1} u \right) \\ \mu_c \dfrac{C}{B_2} \left(1 - \dfrac{\sigma_2}{B_2} u \right) \end{cases} \tag{16}$$

Most of the standard general theorems for the existence of optimal controls such as Filippov (1962), Neustadt (1963) and Fleming and Rishel (1975) require the set of velocities, in this case $F([u_{\min}, u_{\max}])$, to be convex.

In our system (4)–(6), the controls enter nonlinearly, which is the most accurate biological model; however, we cannot ensure existence of optimal controls. Fortunately, due to the magnitude of the parameters $\frac{\sigma_i}{B_i}$ for $i = 1, 2$ and the size of the control u, the linearization $\tilde{F}(u)$ of $F(u)$ about 0 is extremely close to the original system; see Fig. 1. Note that the linearization $\tilde{F}(u)$ about $\frac{u_{\min} + u_{\max}}{2}$ would be even closer. However for easier readability, we choose to use the linearization about 0, which is already very close.

Because the rods and cones are an order of magnitude apart in healthy conditions with rods to cones 30:1 in mice and 20:1 in humans, we do not use the Euclidean distance but instead report the errors for rods and cones separately. These distances are less than 10% error and less than 1% error respectively (Table 2). Because the control terms are of the form $\frac{A}{B+Cu}$, the derivatives don't change sign between $u_{\min}$ and $u_{\max}$ and so the maximum distance is at the endpoints. This shows that the control found for the nonlinear system must be very similar to the optimal control that exists.

	R_n	C
$F(u_{\min})$	7.77e5	2.31e4
$\tilde{F}(u_{\min})$	7.30e5	2.17e4
% Error	6.09%	6.29%
$F(u_{\max})$	9.433e5	2.814e4
$\tilde{F}(u_{\max})$	9.425e5	2.812e4
% Error	0.075%	0.078%

Table 2 Percent error for R_n and C for $F(u)$ and $\tilde{F}(u)$

Percent error is taken separately for rods and cones, because in healthy conditions, they are an order of magnitude apart. Percent errors are taken at the endpoints; see Fig. 1a, b

And, in the results that follow, it is shown that the optimal control for the linearized system is indeed very similar.

3 Optimal Control

3.1 Objective Functional

Next the objective functional is defined for both the nonlinear (4)–(6) and linearized (11)–(13) control models. This optimal control problem is formulated to take into account the administration of RdCVFL to the cones because of the fact that the secondary death of cones is a result of being exposed to oxidative stress and the inclusion of RdCVFL protects from that stress. While using the cumulative portion of full length of cone outer segments, to maximize cone longevity the objective functional also takes care to minimize the dosage of RdCVFL to the cones. The control is denoted by the function $u: [0, t_f] \to [0, 1]$ and is a representation of the percentage of RdCVFL which is administered to assist in cone survival over the time period $[0, t_f]$. This optimal control problem will be compared to experimental results from Elachouri et al. (2015) and thus the dosage u will be considered as being administered over the course of ten days. The objective functional is defined as

$$I(u) = \int_0^{t_f} \left(\frac{\epsilon}{2} (u(t))^2 - (\alpha_1 R_n + \alpha_2 C) \right) dt \qquad (17)$$

where the importance of minimizing u is represented as the weight ϵ and the set of controls is defined as

$$U = \{u | u \text{ is measurable}, u_{\min} \leq u(t) \leq u_{\max}, \ t \in [0, t_f]\} \qquad (18)$$

and this set is closed. The set U is an interval, and hence it is convex. Note that $u_{\min} = 0, u_{\max} = 0.9$ to allow for flexibility in efficiency.

3.2 Existence of Unique Global Solutions for the Nonlinear System

Theorem 1 *For every fixed measurable control $u : [0, t_f] \mapsto [u_{\min}, u_{\max}]$ and every initial condition (R_{n0}, C_0, T_0) in $\bar{\Omega} = \{(R, C, T) : R \geq 0, C \geq 0, T \geq 0\}$, the system defined in* (4)–(6) *has a locally unique and bounded solution defined on $[0, t_f]$.*

Proof By hypothesis, the controls are bounded and measurable functions of time t. For every fixed (R_n, C, T) and fixed control $u(\cdot)$, the right hand side f is a measurable function of time, as a composition of a measurable function and a continuous function in the "good" order (Royden and Fitzpatrick 1988). For each fixed t, the vector field $f(\cdot, u(t))$ is a rational function of (R_n, C, T) without any singularities in the closed first octant, and hence is locally Lipschitz continuous on this set. Using the boundedness of the controls, one can show analogously to Theorem 6 (see "Appendix A") that solutions for this u stay bounded and are thus defined for all positive times t less than or equal to t_f. The calculations are the same, except in (39), the term $\delta_r R_n$ is replaced with $u_{\max}\sigma_1$, and $\delta_c C$ is replaced with $u_{\max}\sigma_2$. By the Carathéodory theorem (Coddington and Levinson 1955 Theorem 1.1), there exists a unique solution on the interval $[0, t_f]$ for this control u.　　□

3.3 Existence of Unique Global Solutions for the Linearized System

Theorem 2 *For every fixed measurable control $u : [0, t_f] \mapsto [u_{\min}, u_{\max}]$ and every initial condition (R_{n0}, C_0, T_0) in $\bar{\Omega} = \{(R, C, T) : R \geq 0, C \geq 0, T \geq 0\}$, the system defined in* (11)–(13) *has a locally unique and bounded solution defined on $[0, t_f]$.*

Proof By hypothesis, the controls are bounded and measurable functions of time t. For every fixed (R_n, C, T) and fixed control $u(\cdot)$, the right hand side f_l is a measurable function of time. For each fixed t, the vector field $f_l(\cdot, u(t))$ is a rational function of (R_n, C, T) without any singularities in the closed first octant, and hence is locally Lipschitz continuous on this set. Using the boundedness of the controls, one can show analogously to Theorem 6 that solutions for this u stay bounded and are thus defined for all positive times t less than or equal to t_f. The calculations are the same, except in (39) the term $\frac{R_n}{B_1 + \delta_r R_n}$ is replaced with $\frac{R_n}{B_1}\left(1 - \frac{\sigma_1}{B_1}u\right)$, and $\frac{C}{B_2 + \delta_c C}$ is replaced with $\frac{C}{B_2}\left(1 - \frac{\sigma_2}{B_2}u\right)$. By the Carathéodory theorem (Coddington and Levinson 1955 Theorem 1.1), there exists a unique solution on the interval $[0, t_f]$ for this control u.　　□

3.4 Existence of Optimal Control for the Linearized System

Because most standard general theorems for the existence of optimal controls require the set of velocities to be convex, we only show the existence of optimal controls for the system (11)–(13) where the controls enter linearly.

We will verify that the optimal control problem (11)–(13) together with the objective functional (17) satisfies the conditions of Theorem 2.2 from Lenhart and Workman (2007) for the basic problem (1.2) (p. 7 of the same reference). To keep this manuscript

self-contained, we paraphrase the statement of that theorem using our terminology and notation, such as noting that the dynamics and cost functional do not explicitly depend on time.

The following theorem refers to the problem of minimizing a cost functional (equation (1.2) in Lenhart and Workman (2007)) $J(u) = \int_0^{t_1} \ell(x(t), u(t)) \, dt$ subject to $x'(t) = f(x(t), u(t))$, $x(0) = x_0$ with f and ℓ continuously differentiable.

Theorem 3 (Lenhart and Workman, paraphrased and customized) *Let the set of controls be Lebesgue measurable on $0 \leq t \leq t_1$ with values in $\mathbb{R}$. Suppose that $f(x, u)$ is convex in u, and there exists constants C_4 and C_1, C_2, $C_3 > 0$, and $\beta > 1$ such that for all $t \in [0, t_1]$, and all x, x_1, $u \in \mathbb{R}$*

$$
\begin{aligned}
&\text{(i)} \quad f(x, u) = \alpha(x) + \beta(x)u, \\
&\text{(ii)} \quad |f(x, u)| \leq C_1(1 + |x| + |u|), \\
&\text{(iii)} \quad |f(x_1, u) - f(x, u)| \leq C_2(|x_1 - x|)(1 + |u|), \quad \text{and} \\
&\text{(iv)} \quad |\ell(x, u)| \geq C_3|u|^\beta - C_4.
\end{aligned}
\tag{19}
$$

Then there exists an optimal control u^* minimizing $J(u)$ with $J(u^*)$ finite.

To verify that this theorem applies to our system, first note that with Corollary 1 and Remark 1 in the appendix, we may restrict our considerations to a compact, forward invariant *simplex S'* in the first octant. On this set, the dynamics $f(x, u)$ is affine in the control u and rational in the state $x = (R, C, T)$ and without singularities in the first quadrant, and thus (i) and (ii) are satisfied. Since f is continuously differentiable it is Lipschitz continuous on the compact set S' with Lipschitz constant independent of the control, and thus (iii) is satisfied. The Lagrangian in the functional (17) clearly is of the form (iv) with $\beta = 2$ and with finite C_4 since the term $(\alpha_1 R_n + \alpha_2 C)$ is linear in the state variables and thus bounded on the domain S' of interest.

3.5 Optimality Conditions

There are first-order necessary optimality conditions which must be met for the optimal control problem that will be outlined in this section. The optimal control problem, subject to the nonlinear state equations (4)–(6) with objective functional $I(u)$ must meet the following conditions in order for the optimal control $u^*(t)$ to be characterized.

The previous equations will be rewritten as the following maximization problem for convenience:

$$
\max_u J(u) \text{ subject to } \dot{x} = f(x, u)
\tag{20}
$$

where

$$
J(u) = -I(u) = \int_0^{t_f} \left(\alpha_1 R_n + \alpha_2 C - \frac{\epsilon}{2} u^2 \right) dt.
\tag{21}
$$

Thus an optimal control u^* must be as follows:

$$J(u^*) = \max_{u \in U} J(u) \text{ subject to } \dot{x} = f(x, u^*). \tag{22}$$

Then continuing to Pontryagin's Maximum Principle, the Hamiltonian is first defined:

$$H(x, \lambda, u) = \alpha_1 R_n + \alpha_2 C - \frac{\epsilon}{2} u^2 + \lambda^T f(x, u) \tag{23}$$

where next, λ is defined as the vector of adjoint variables, which are represented as $\lambda \equiv \lambda(t) = (\lambda_1(t), \lambda_2(t), \lambda_3(t))^T$. Then we let $H \equiv H(x, \lambda, u)$ and $\lambda_i \equiv \lambda_i(t)$ with $i = 1, \ldots, 3$ for convenience.

Nonlinear System

Even though an optimal control is not guaranteed to exist, we proceed with the standard technique for finding one and then compare with the linear version. The optimal control that we find given the standard procedure will be referred to as the putative optimal control.

Using the nonlinear system (4)–(6) and the objective function, the Hamiltonian is defined as follows:

$$
\begin{aligned}
H = {} & \alpha_1 R_n + \alpha_2 C - \frac{\epsilon}{2} u^2 \\
& + \lambda_1 \left(R_n T a_n - \mu_n \left(\frac{R_n}{B_1 + u\sigma_1} \right) \right) \\
& + \lambda_2 \left(v_2 \left(\frac{V_{\max}(\delta_n R_n)^2}{K_{mg}^2 + (\delta_n R_n)^2} + p \right) CT - \mu_c \left(\frac{C}{B_2 + u\sigma_2} \right) \right) \\
& + \lambda_3 \left(T \left(\Gamma - kT - \beta_n R_n - \gamma C \right) \right)
\end{aligned}
\tag{24}
$$

Theorem 4 *Pontryagin's Maximum Principle: If u^* and $x^* = (R_n^*, C^*, T^*)$ are optimal for problem (22) then there exist absolutely continuous and piecewise differentiable adjoint functions $\lambda_i : [0, t_f] \to \mathbb{R}$ for $i = 1, 2, 3, 4$ such that*

$$
\begin{aligned}
\frac{\partial \lambda_1}{\partial t} = {} & -\frac{\partial H}{\partial R_n}(x^*, u^*) = -\alpha_1 - \lambda_1 \left(T^* a_n - \frac{\mu_n}{B_1 + u\sigma_1} \right) + \lambda_3 \beta_n T^* \\
& - \lambda_2 \left(v_2 \left(\frac{2 K_{mg}^2 V_{\max} \delta_n^2 R_n^*}{(K_{mg}^2 + (\delta_n R_n^*)^2)^2} \right) C^* T^* \right)
\end{aligned}
\tag{25}
$$

$$
\begin{aligned}
\frac{\partial \lambda_2}{\partial t} = {} & -\frac{\partial H}{\partial C}(x^*, u^*) = -\alpha_2 + \lambda_3 \gamma T^* \\
& - \lambda_2 \left(v_2 \left(\frac{V_{\max}(\delta_n R_n^*)^2}{K_{mg}^2 + (\delta_n R_n^*)^2} + p \right) T^* - \frac{\mu_c}{B_2 + u\sigma_2} \right)
\end{aligned}
\tag{26}
$$

$$\frac{\partial \lambda_3}{\partial t} = -\frac{\partial H}{\partial T}(x^*, u^*) = -\lambda_1 R_n^* a_n - \lambda_3 (\Gamma - 2\kappa T^* - \beta_n R_n^* - \gamma C^*)$$
$$- \lambda_2 \left(v_2 \left(\frac{V_{\max}(\delta_n R_n^*)^2}{K_{mg}^2 + (\delta_n R_n^*)^2} + p \right) C^* \right). \tag{27}$$

The costate λ satisfies the transversality conditions being

$$\lambda_i(t_f) = 0, \ for \ i = 1, \ldots, 3.$$

For all $t \in [t_0, t_f]$, the optimal control $u^*(t)$ maximizes the Hamiltonian, i.e.
$\forall u \in [u_{\min}, u_{\max}], \ H(x^*(t), \lambda(t), u^*(t)) \geq H(x^*(t), \lambda(t), u).$

Linearized System

For the linearized system (11)–(13), the Hamiltonian is defined as follows:

$$H = \alpha_1 R_n + \alpha_2 C - \frac{\epsilon}{2} u^2$$
$$+ \lambda_1 \left(R_n T a_n - \mu_n \frac{R_n}{B_1} \left(1 - \frac{\sigma_1}{B_1} u \right) \right)$$
$$+ \lambda_2 \left(v_2 \left(\frac{V_{\max}(\delta_n R_n)^2}{K_{mg}^2 + (\delta_n R_n)^2} + p \right) CT - \mu_c \frac{C}{B_2} \left(1 - \frac{\sigma_2}{B_2} u \right) \right)$$
$$+ \lambda_3 (T (\Gamma - kT - \beta_n R_n - \gamma C)) \tag{28}$$

Theorem 5 *Pontryagin's Maximum Principle: If u^* and $x^* = (R_n^*, C^*, T^*)$ are optimal for problem (22) then there exist absolutely continuous and piecewise differentiable adjoint functions $\lambda_i : [0, t_f] \to \mathbb{R}$ for $i = 1, 2, 3, 4$ such that*

$$\frac{\partial \lambda_1}{\partial t} = -\frac{\partial H}{\partial R_n}(x^*, u^*) = -\alpha_1 - \lambda_1 \left(T^* a_n - \frac{\mu_n}{B_1} \left(1 - \frac{\sigma_1 u}{B_1} \right) \right) + \lambda_3 \beta_n T^*$$
$$- \lambda_2 \left(v_2 \left(\frac{2 K_{mg}^2 V_{\max} \delta_n^2 R_n^*}{(K_{mg}^2 + (\delta_n R_n^*)^2)^2} \right) C^* T^* \right) \tag{29}$$

$$\frac{\partial \lambda_2}{\partial t} = -\frac{\partial H}{\partial C}(x^*, u^*) = -\alpha_2 + \lambda_3 \gamma T^*$$
$$- \lambda_2 \left(v_2 \left(\frac{V_{\max}(\delta_n R_n^*)^2}{K_{mg}^2 + (\delta_n R_n^*)^2} + p \right) T^* - \frac{\mu_c}{B_2} \left(1 - \frac{\sigma_2 u}{B_2} \right) \right) \tag{30}$$

$$\frac{\partial \lambda_3}{\partial t} = -\frac{\partial H}{\partial T}(x^*, u^*) = -\lambda_1 R_n^* a_n - \lambda_3 (\Gamma - 2\kappa T^* - \beta_n R_n^* - \gamma C^*)$$
$$- \lambda_2 \left(v_2 \left(\frac{V_{\max}(\delta_n R_n^*)^2}{K_{mg}^2 + (\delta_n R_n^*)^2} + p \right) C^* \right). \tag{31}$$

The costate λ satisfies the transversality conditions being

$$\lambda_i(t_f) = 0, \ for \ i = 1, \ldots, 3.$$

For all $t \in [t_0, t_f]$, *the optimal control* $u^*(t)$ *maximizes the Hamiltonian, i.e.* $\forall\, u \in [u_{\min}, u_{\max}],\; H(x^*(t), \lambda(t), u^*(t)) \geq H(x^*(t), \lambda(t), u)$.

3.6 Description of the Discretized Variables

In this section an approximate solution to the system of equations (4)–(6), $\vec{x}$, is described. The following nodes describe how the time interval $[0, t_f]$ is discretized into N subintervals that are equally spaced with

$$h = t_{i+1} - t_i, \text{ for } i = 0, \ldots, N - 1,$$

and

$$0 = t_0 < t_1 < \cdots < t_N = t_f. \tag{32}$$

Next, the discretized vector $\vec{x}$ at time t_k is defined as

$$\vec{x_k} = (R_n(t_k), C(t_k), T(t_k))^T.$$

It follows similarly that for $k = 0, \ldots, N$, $u_k = u(t_k)$ and for all time steps t_k with $k = 0, 1, 2, \ldots N$, all discretized values are contained in the vector $\vec{u} = [u_0, u_1, u_2, \ldots, u_N]$.

Next, an approximation to the solution of the system of equations (4)–(6) for the state variable $\vec{x}$ is calculated given initial conditions $x_0 \in R^3$ with initial $\vec{u}$ over the time interval $[0, t_f]$, by implementing the fourth-order Runge–Kutta method forward in time with $k = 0, \ldots, N$. The forward Runge–Kutta method is as follows:

$$\vec{k}_1 = \vec{f}(t_k, \vec{x}_k, u_k)$$
$$\vec{k}_2 = \vec{f}\left(t_k + \frac{h}{2}, \vec{x}_k + \frac{h}{2}\vec{k}_1, \frac{1}{2}(u_k + u_{k+1})\right)$$
$$\vec{k}_3 = \vec{f}\left(t_k + \frac{h}{2}, \vec{x}_k + \frac{h}{2}\vec{k}_2, \frac{1}{2}(u_k + u_{k+1})\right)$$
$$\vec{k}_4 = \vec{f}\left(t_{k+1}, \vec{x}_k + \vec{k}_3, u_{k+1}\right)$$
$$\vec{x}_{k+1} = \vec{x}_k + \frac{h}{6}\left(\vec{k}_1 + 2\vec{k}_2 + 2\vec{k}_3 + \vec{k}_4\right).$$

It is important to note that there are several different ways to approximate the value of u_k in calculating $\vec{k}_2$ and $\vec{k}_3$. In this algorithm, we replace u_k with the average, $\frac{1}{2}(u_k + u_{k+1})$, because this has been shown to be sufficient (Lenhart and Workman 2007).

Next, the Runge–Kutta method is implemented backward in time to numerically solve the adjoint system and compute the solution λ. The definitions of h and discretization of the time variable $t \in [0, t_f]$ remains the same as stated previously. Define the adjoint vector $\vec{\lambda}_k \in \mathbb{R}^3$, for which the values of the adjoint variables at

each discrete time t_k are the components, as $\vec{\lambda}_k = (\lambda_1(t_k), \lambda_2(t_k), \lambda_3(t_k))^T$. The initial iterate is set to $\vec{\lambda}_N = 0$ in order to enforce the transversality condition. Then, the backward solve Runge-Kutta method is as follows for $k = N, N-1, \ldots, 1$:

$$\vec{k}_1 = \vec{g}\left(t_k, \vec{\lambda}_k, \vec{x}_k, u_k\right)$$

$$\vec{k}_2 = \vec{g}\left(t_k - \frac{h}{2}, \vec{\lambda}_k - \frac{h}{2}\vec{k}_1, \frac{1}{2}(\vec{x}_k + \vec{x}_{k-1}), \frac{1}{2}(u_k + u_{k-1})\right)$$

$$\vec{k}_3 = \vec{g}\left(t_k - \frac{h}{2}, \vec{\lambda}_k - \frac{h}{2}\vec{k}_2, \frac{1}{2}(\vec{x}_k + \vec{x}_{k-1}), \frac{1}{2}(u_k + u_{k-1})\right)$$

$$\vec{k}_4 = \vec{g}\left(t_{k-1}, \vec{\lambda}_k - \vec{k}_3, \vec{x}_{k-1}, u_{k-1}\right)$$

$$\vec{\lambda}_{k-1} = \vec{\lambda}_k - \frac{h}{6}\left(\vec{k}_1 + 2\vec{k}_2 + 2\vec{k}_3 + \vec{k}_4\right).$$

3.7 Updating the Control Variable

Nonlinear System

Next, the characterization of the optimal control is derived using Pontryagin's Maximum Principle. By this principle, the Hamiltonian must satisfy

$$\frac{\partial H}{\partial u} = 0 = -\epsilon u + \frac{\lambda_1 \mu_n \sigma_1 R_n}{(B_1 + u\sigma_1)^2} + \frac{\lambda_2 \mu_c \sigma_2 C}{(B_2 + u\sigma_2)^2} \tag{33}$$

at optimality. Rearranging gives

$$\epsilon u = \frac{\lambda_1 \mu_n \sigma_1 R_n}{(B_1 + u\sigma_1)^2} + \frac{\lambda_2 \mu_c \sigma_2 C}{(B_2 + u\sigma_2)^2}, \tag{34}$$

where we observe that since all the parameters in (34) are positive, there will be only one intersection of ϵu with the right-hand-side, and this intersection will occur in the first quadrant. However, solving for u, and only taking the unique real root of (33), the analytic solution is too cumbersome to enter into MATLAB, and so it is solved for using a root finding method. Then, u becomes the average of the new value u and the old value for u, for each time step k.

Then, a new vector of control variables, $\vec{u} = [u_0, u_1, u_2, \ldots, u_N]$, is formed to test convergence once all the values over the discretized time interval $[0, t_f]$ have been calculated.

Linearized System

Now for the linearized system the characterization of the optimal control is derived using Pontryagin's Maximum Principle. For this system, the Hamiltonian must satisfy

$$\frac{\partial H}{\partial u} = 0 = -\epsilon u + \frac{\lambda_1 \mu_n \sigma_1 R_n}{B_1^2} + \frac{\lambda_2 \mu_c \sigma_2 C}{B_2^2} \tag{35}$$

at optimality.

Solving for u, we get

$$u = \frac{\lambda_2 \mu_c C \sigma_2 B_1^2 + \lambda_1 \mu_n R_n \sigma_1 B_2^2}{B_1^2 B_2^2 \epsilon}. \tag{36}$$

Then, u becomes the average of the new value u and the old value for u, for each time step k. After that, a new vector of control variables, $\vec{u} = [u_0, u_1, u_2, \ldots, u_N]$, is formed to test convergence once all the values over the discretized time interval $[0, t_f]$ have been calculated. We observe that Taylor expanding the nonlinear terms in the characterization of u for the nonlinear equations and keeping linear terms, (33), gives the exact same characterization as (36).

3.8 The Forward-Backward Sweep Method (FBSM)

3.8.1 FBSM Algorithm

The numerical approximation of the optimality condition can be summarized by the following algorithm (Lenhart and Workman 2007). Assume that the initial condition is given as $\vec{x}(t_0)$, over the uniformly discretized time interval $[0, t_f]$ with mesh size h and stopping criteria given by δ.

1. Initialize $\vec{u} = 0$.
2. Approximate solution $\vec{x}$ to (ODE) forward in time t over time interval $[0, t_f]$ using $\vec{u}$ and $\vec{x}(t_0)$.
3. Approximate solution $\vec{\lambda}$ to (ADJ) backward in time t over $[0, t_f]$ using $\vec{u}, \vec{x}(t_0)$ and $\vec{\lambda}(t_f) = 0$.
4. Update $\vec{u}$ using the characterization formula, equation (34) for the nonlinear system or (36) for the linear system.
5. Test for convergence. If convergence is not met, return to 2. and repeat steps 2–5 using the updated values for $\vec{u}$ and $\vec{x}(t_0)$.

Each single iteration is defined as each single completion of steps 2–5. When approximating solutions numerically for optimal control problems, this algorithm is the standard procedure; however, it has limitations (Lenhart and Workman 2007). It is also important to note that the solutions do not always converge following FBSM (McAsey et al. 2012). General assumptions under which this algorithm converges are defined in McAsey et al. (2012), and the authors also analyze an example of an optimal control problem for which there is a known analytical solution (Lenhart and Workman 2007), yet for which after 1000 iterations there is still no convergence. The magnitude of the coefficient of a term in the objective functional to the length of the time interval is what this nonconvergence is attributed to by the authors. Figure 2 shows the convergence for nonlinear and linearized models.

3.8.2 Stopping Criteria for the FBSM

The following discretization of $\vec{u} \equiv \vec{u}(t) \in \mathbb{R}^{N+1}$ over the discretization of time $[0, t_f]$ holds the estimated values for the Forward-Backward Sweep Method (FBSM) for each current iteration:

$$\vec{u} = (u(t_0), u(t_1), u(t_2), \ldots, u(t_f)).$$

It follows that the estimated values of u from the previous iteration of FBSM is defined as $\vec{u}_{old} \in \mathbb{R}^{N+1}$. See, for example, Lenhart and Workman (2007).

Once the estimated values of u are calculated at each iteration, a stopping criteria must be met for FBSM using relative errors for the control, state variables, and adjoint variables. This implementation is now demonstrated using a given tolerance δ and the values for the control u as an example that covers the other variables listed in general. The relative error δ is now defined in terms of the control u and the ℓ_1 vector norm:

$$\frac{||\vec{u} - \vec{u}_{old}||}{||\vec{u}||} \leq \delta,$$

which can be rewritten as the following in order to take into account the fact that the control variable may have the value 0:

$$\delta ||\vec{u}|| - ||\vec{u} - \vec{u}_{old}|| \geq 0. \tag{37}$$

Next, β_1 is defined following the work done by Lenhart and Workman (2007):

$$\beta_1 = \delta ||\vec{u}|| - ||\vec{u} - \vec{u}_{old}||.$$

Now, for each current iteration of the FBSM method, the relative errors for each of the state variables can be rewritten. The state variables defined as $\vec{X} = (\vec{X}_1, \vec{X}_2, \vec{X}_3)^T \in \mathbb{R}^{3 \times (N+1)}$. These relative errors which are obtained from the current iteration are given in the matrix:

$$\vec{X} = \begin{pmatrix} \vec{X}_1 \\ \vec{X}_2 \\ \vec{X}_3 \end{pmatrix} = \begin{pmatrix} x_1(t_0) & x_1(t_1) & x_1(t_2) & \cdots & x_1(t_f) \\ x_2(t_0) & x_2(t_1) & x_2(t_2) & \cdots & x_2(t_f) \\ x_3(t_0) & x_3(t_1) & x_3(t_2) & \cdots & x_3(t_f) \end{pmatrix}$$

For each previous iteration of FBSM, the estimated state variables are also stored, in a matrix that is constructed in the same fashion as $\vec{X}$. This matrix is defined as $\vec{X}_{old} \in \mathbb{R}^{3 \times (N+1)}$ with the difference being that the ith row is denoted by $\vec{X}_{old_i}$ instead of $\vec{X}_i$. This ith row is defined as follows for both of these matrices:

$$\beta_{i+1} = \delta ||\vec{X}_i|| - ||\vec{X}_i - \vec{X}_{old_i}||, \quad i = 1, \ldots, 3.$$

Next, the adjoint variables, defined as $\vec{\lambda}_i$, $i = 1, \ldots, 3$, must be taken into consideration and the process must be repeated for them. The estimated values of adjoint variables are similarly calculated using the current iteration of FBSM, which are then stored in the matrix $\Lambda = (\Lambda_1, \Lambda_2, \Lambda_3)^T \in \mathbb{R}^{4 \times (N+1)}$. Once again, $\Lambda_{old} \in \mathbb{R}^{3 \times (N+1)}$ is a matrix created using the previously estimated values of FBSM from the last iteration, and it follows that

$$\beta_{i+1} = \delta ||\Lambda_i|| - ||\Lambda_i - \Lambda_{old_i}||, \quad i = 4, \ldots, 6.$$

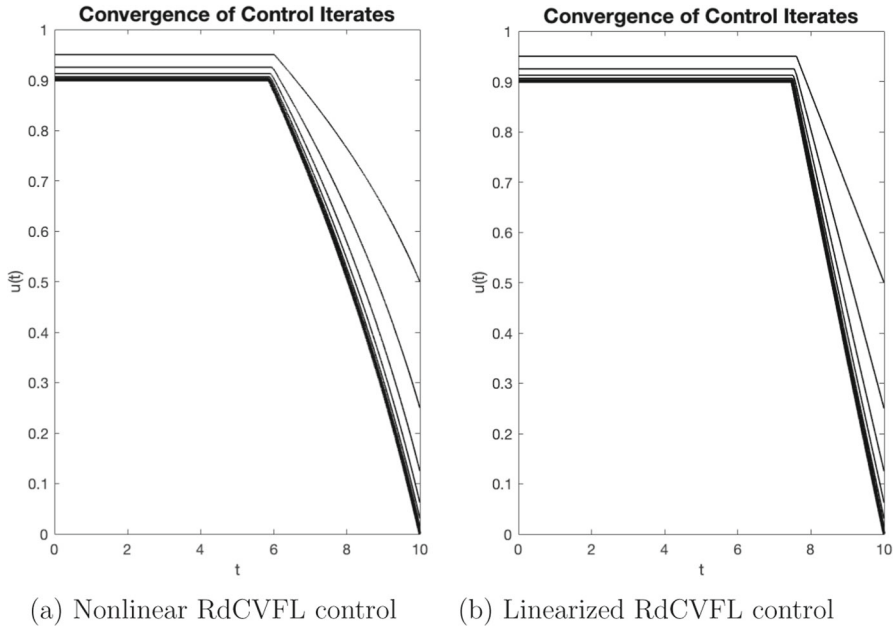(a) Nonlinear RdCVFL control   (b) Linearized RdCVFL control

Fig. 2 Plots of the control iterates for the RdCVFL control models with $\epsilon = 7e5$. **a** Plot of the control estimates for the nonlinear model with control (4)–(6). Recall that for this case, we do not have proof of existence of optimal control. However, for the sake of comparison and biological relevance, we follow the same methods to find u^*, which we call the putative optimal control in this instance. The putative optimal control u^* is depicted by the bold line. Observe that the control iterates converge to u^*, which is achieved in 12 iterations. **b** Plot of the control estimates for the linearized model with control (11)–(13). In this case, we do have a mathematical proof of existence for the optimal control. The optimal control u^* is depicted by the bold line. Observe that the control iterates converge to u^*, which is achieved in 12 iterations

Then, the following is obtained:

$$\{\beta_1, \beta_2, \ldots, \beta_7\}.$$

Next, for the stopping criteria to be met in order to obtain convergence, the following must hold:

$$\min\{\beta_1, \beta_2, \ldots, \beta_7\} > 0,$$

and if this inequality holds, then convergence has been obtained and the process is halted. If the stopping criteria has not been met, then the process is repeated with an additional run through the FBSM method.

4 Numerical Results of Control Applied to Rods and Cones with RdCVFL

Our nonlinear model (4)–(6) is based on the experimental results from Elachouri et al. (2015) for the *Nxnl1-/-* mouse. While we don't have a mathematical proof

Table 3 Parameters for E_5 stability; the estimated parameters result in E_5 stability at a reasonable level; see Wifvat et al. (2021)

Variable	Value	Units	Citation
a_n	1.25e−06	$\frac{1}{\text{day mM}}$	Estimated
β_n	2.0e−07	$\frac{1}{\text{day (rod OS)}}$	Estimated
γ	5.0e−5	$\frac{1}{\text{day (cone OS)}}$	Estimated
Γ	430.0	$\frac{1}{\text{day}}$	Estimated
κ	5.0e−3	$\frac{1}{\text{day mM}}$	Estimated
μ_n	106.0	$\frac{\text{mM}}{\text{day}}$	Estimated
μ_c	135.0	$\frac{\text{mM}}{\text{day}}$	Estimated
K_m	19	mM	Carruthers (2016)
B_1	1000	mM	Estimated
B_2	1200	mM	Estimated
$V_{\max}$	1728	$\frac{\text{mM}}{\text{day}}$	Carruthers (2016)
δ_n	6.5e−5	mM	Léveillard et al. (2004)
δ_r	1.0e−6	mM	Estimated
δ_c	1.0e−4	mM	Estimated
ν_2	7.65e−10	$\frac{1}{\text{mM}^2}$	Estimated
p	1.0e−3	$\frac{\text{mM}}{\text{day}}$	Estimated

for existence of the optimal control, this experiment shows a decrease in rods and cones over the course of 10 days, with long term behavior approaching E_2, where all the rods and cones have died off while the nutrients remain. Table 3 gives the parameter values that fit the data and give E_5 stable, with B_1, B_2, δ_r and δ_c from (1)–(3) having altered values to reflect the case of mice that do not have RdCVFL and have experienced light damage, where we consider *Nxnl1* to be a proxy for RdCVFL (Table 4). The α-values are relative weights compared with each other and, in our case, chosen to match the experimental data of the degeneration of R_n and C. The values for α were chosen to be $\alpha_1 = 1$ and $\alpha_2 = 1.2$ to show the weights of control for rods and cones, respectively. Recall that the values for σ_1 is 192, which is $\delta_r R_{n0}$ rounded to the nearest whole number, and σ_2 is 234, $\delta_c C_0$ rounded to the nearest whole number. The lack of RdCVFL is illustrated by the δ_r and δ_c values being set equal to zero, and the light damage is reflected in the lowered values of B_1 and B_2. The numerical results show that with an ϵ value of 7.0e5 in (21), the numerical results agree with the experimental data; see Fig. 3. This shows that the progression of retinal diseases such as RP may be slowed using treatments that involve RdCVFL.

With the linearized control model (11)–(13), and using the same values for all the parameters and initial conditions, there is a higher saving rate but adjusting ϵ to be 1.8E+6, the savings rate is similar to the results of the nonlinear version.

Table 4 Parameters changed for -/- LD; the estimated parameters give agreement with the degeneration observed in Elachouri et al. (2015)

Variable	Value	Units	Citation
B_1	700	mM	Estimated
B_2	840	mM	Estimated
δ_r	0	mM	Elachouri et al. (2015)
δ_c	0	mM	Elachouri et al. (2015)
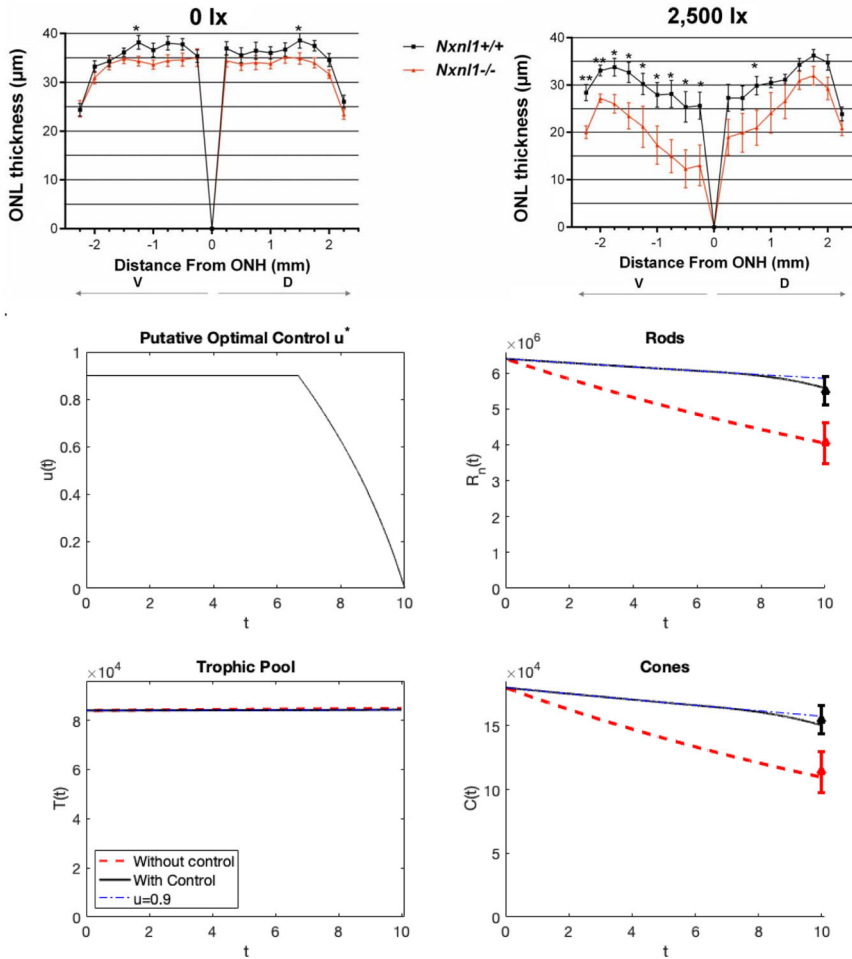
Fig. 3 (Color figure online) The results of decay of both cones and rods, for the nonlinear RdCVFL control model (4)–(6). The initial conditions are $R_n = 6.4e6$, $C = 1.8e5$, $T = 8e4$, over the course of 10 days (reflected by the experimental results of Elachouri et al. (2015) for the *Nxnl1*-/- mouse, presented in the top panel), without control compared to the results of adding control to the rods and cones. The data points at time $t = 10$ for the rods and cones are from experimental results of Elachouri et al. (2015)
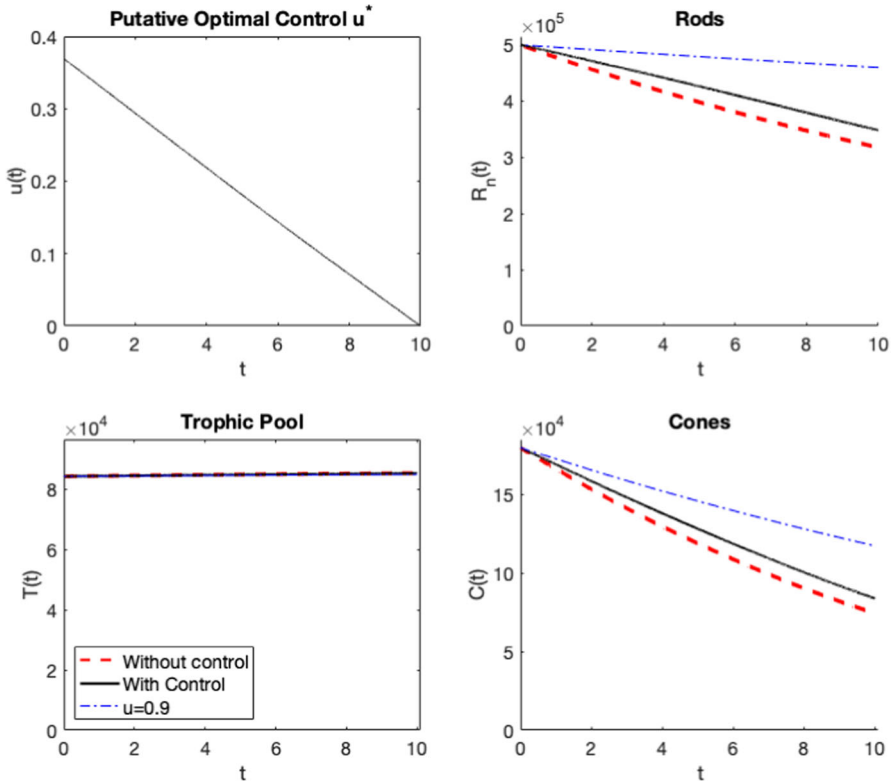
Fig. 4 (Color figure online) The results of decay of both cones and rods, for the nonlinear RdCVFL control model (4)–(6). The initial conditions are $R_n = 0.5e6$, $C = 1.8e5$, $T = 8e4$, a smaller value of the R_n initial condition only, over the course of 10 days (reflected by the experimental results of Elachouri et al. (2015) for the *Nxnl1-/-* mouse), without control compared to the results of adding control to the rods and cones. Note that no experimental results are available for treatment with RdCVFL for these initial conditions (so there are no data points at $t = 10$ as there were in Fig. 3)

5 Sensitivity Analysis

Next in order to see more clearly how the addition of the control impacts the rest of the model and the other parameters in the model, a sensitivity analysis is performed. The PRCC method is used in order to do a global sensitivity analysis and see which parameters have the strongest effects, and understand how variation in the parameter values affects the outcomes of our biological system. We first analyze the model without control (1)–(3), the nonlinear RdCVFL control model (4)–(6) and the linearized RdCVFL control model (11)–(13). Using the initial conditions presented in the control results in Fig. 3, $R_n = 6.4e6$, $C = 1.8e5$, $T = 8e4$, we see from Fig. 5a–d the difference between the photoreceptor PRCC values without control (a)–(b), and with control (c)–(d). When there is not a control added to the model, the initial values of the state variables for rods and cones are important. However, when there is control added, these initial values are no longer significant. Notice that with or without con-

trol, the values B_1 and B_2 are significant. These parameters are correlated to the ROS, which RdCVFL has been experimentally shown to counteract. Similarly, the amount of RdCVFL present also affects shedding rates, which are represented by μ_n and μ_c, which also show strong significance. Notice also that the quantities

$$D_T = \frac{\Gamma}{\kappa}, \, D_n = \frac{\mu_n}{a_n} \tag{38}$$

are also significant, because the related parameters Γ, κ, μ_n and a_n are all significant as well. These quantities are important because they have been shown in previous mathematical work (Camacho et al. 2016, ?) to be key ratios that determine the stability of the equilibria. This shows that even in the case where RdCVFL is not present, key factors relating to energy uptake and the metabolic processes which are affected by RdCVFL are still significant.

For the initial values $R_n = 0.5\text{e}6, C = 1.8\text{e}5, T = 8\text{e}4$, which are the initial conditions in the control model shown in Fig. 4, all of the PRCC plots are the same for both the nonlinear model without control (1)–(3), the nonlinear control model (4)–(6) and the linearized control model (11)–(13) except for four cases which are shown in Fig. 6. Only for the cones, we can see that several parameters are now more significant. For cones in the nonlinear model without control (1)–(3), the initial value of the rods is now significant, along with a, δ_n, μ_n, K_m and B_1. Then for the nonlinear control model, the new significant parameters are a, δ_n, K_m and B_1. For the linearized control model, when $\epsilon = 7\text{e}5$, which is the same ϵ that's used for the nonlinear control model, the newly significant parameters are a, δ_n, μ_n and K_m. Finally, when we use the ϵ value that is needed to get similar results from the linear control model as the nonlinear control model, $\epsilon = 1.8e6$, we see the same significant parameters as for the previous ϵ value, except now B_1 is also significant as well. Additionally, the PRCC plots were also tested at the initial values $R_n = 3.6\text{e}6, C = 1.8\text{e}5, T = 8\text{e}4$ and the results were the same as for the first initial values $R_n = 6.4\text{e}6, C = 1.8\text{e}5, T = 8\text{e}4$ for both the rods and the cones.

6 Conclusion

This is the first mathematical optimal control model of a light damaged retina and the potential effects of RdCVFL treatment. The RdCVFL control terms are non-linear for biological accuracy but this results in the standard general theorems for existence of optimal controls failing to apply. We show the close agreement of the original model with the linearization of the control terms in the model and prove existence of an optimal control for the linearized model in Sect. 2. Because of this close agreement, we proceed under the assumption that a numerical optimal control obtained algorithmically and numerically may accurately represent an optimal control of the nonlinear system. The parameters are fit to real world experimental data for *Nxnl1-/-* mice, and the results show a savings rate for rods and cones that agrees with experimental data. Similar results are obtained with the linear system by choosing a different ϵ. We conclude that with the presence of RdCVFL added to

(a) PRCC plot for rods -/- LD, (1)–(3)

(b) PRCC plot for cones -/- LD, (1)–(3)

(c) PRCC plot for rods -/- LD, (4)–(6)
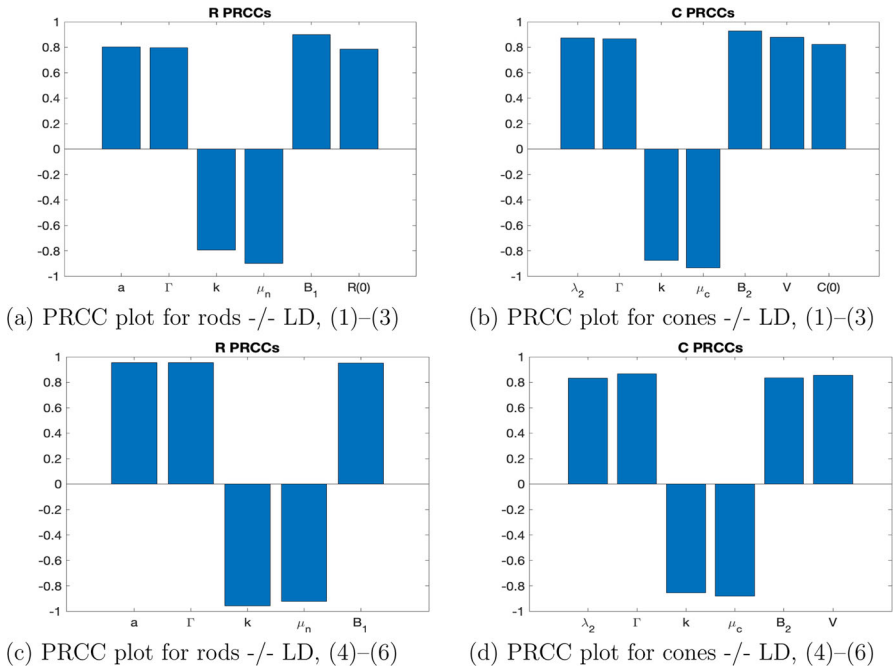

(d) PRCC plot for cones -/- LD, (4)–(6)

Fig. 5 (Color figure online) **a, b** PRCC plots taken at 10 days for rods and cones, respectively, for the -/- mouse with LD for the model without control (1)–(3). The parameters are in Table 3 except the four changed parameters in Table 4. The **c, d** PRCC plots taken at 10 days for rods and cones, respectively, for the -/- mouse under the same conditions except now with nonlinear RdCVFL control u added (4)–(6). The difference is that the initial population of the state variable is no longer significant. Note that this is for the nonlinear model (4)–(6) with initial conditions $R_n = 6.4e6$, $C = 1.8e5$, $T = 8e4$. See Fig. 3 for the control plot. The linearized control model (11)–(13) has the same qualitative results as shown in (**c, d**)

the model of a diseased retina without any naturally occurring RdCVFL, the photoreceptor death is greatly reduced. In fact, it is potentially possible to retain the same amount of vision as a healthy eye, which is reflected in the control model reaching the same population levels as the experimental data of the nondiseased eye. This is an optimistic result for the further study of RdCVFL treatment in human trials.

Further, a global sensitivity and uncertainty analysis was performed to understand what the affect is of each input on the variability of the output of the model. This analysis of the control model was compared to the model without control to understand the differences which occur when control is added to the model. Without control, the PRCC plots show the significant parameters that affect the model output the most. These are the initial values $R(0)$, $C(0)$, the shedding rates and cell metabolism μ_n, μ_c, as well as other uptake and renewal factors such as a, Γ and κ. The only difference when this analysis is performed on the optimal control model, is that the initial values $R(0)$, $C(0)$ are no longer significant. All models showed similar qualitative results for the listed initial conditions, meaning that it is especially important to look into
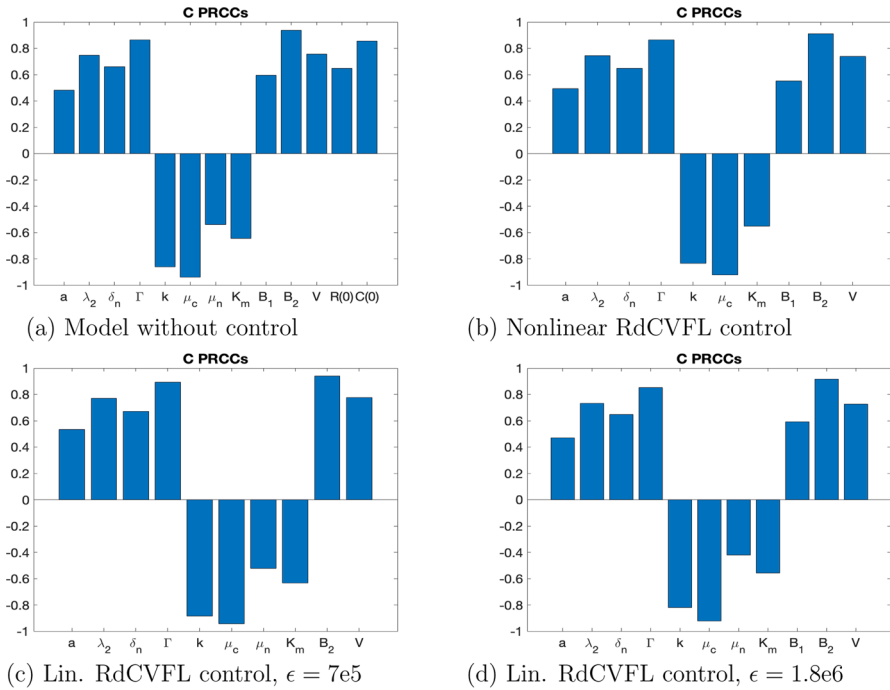
Fig. 6 a–d PRCC plots taken at 10 days for cones, for the -/- mouse with LD and initial conditions $R_n = 0.5e6$, $C = 1.8e5$, $T = 8e4$. The **a** is for the nonlinear model without control (1)–(3) and **b** is for the nonlinear control model (4)–(6). The **c, d** the PRCC plots for the linearized model with control (11)–(13) where **c** has the same ϵ value as the nonlinear model, $\epsilon = 7e5$ and **d** has $\epsilon = 1.8e6$. We observe that the qualitative results of the nonlinear and linearized models, **b, d** respectively, are similar and note that we considered 0.4 to be the value for statistical significance in the PRCC plots

these significant parameters. These results show that the potential RdCVFL treatment may still be able to take effect and help save the remaining photoreceptor population, even with a small initial population of photoreceptors. This is important because many individuals who suffer from RP do not attain a diagnosis or treatment until the disease has already progressed and affected their vision somewhat. Thus it is hopeful that for all patients, there can still be some saving effect for what vision is left.

Based on both the optimal control and the sensitivity and uncertainty analysis, RdCVFL is shown to be an important factor for the survival of photoreceptor populations. In retinas that do not have RdCVFL being produced, a treatment involving RdCVFL may be able to help patients retain vision and slow the progression of the disease. Based on the sensitivity and uncertainty results, this type of potential treatment shows promise for helping at any stage of such retinal diseases. Overall, RdCVFL has been shown to be an important factor in helping the retinas maintain photoreceptor survival and may potentially help patients retain vision.

A Positivity and Boundedness of Solutions

A.1 Existence of Unique Global Solutions for the System without Control

Theorem 6 *There exist locally unique solutions to the initial value problems of the system of equations defined in (1)–(3) for ($R(0) = R_{n_0}$, $C(0) = C_0$, $T(0) = T_0$) in $\mathbb{R}^3$ where $R_{n0} \neq \frac{-B_1}{\delta_r}$ and $C_0 \neq \frac{-B_2}{\delta_c}$. The coordinate planes and hence the positive octant $\Omega = \{(R, C, T) : R > 0, C > 0, T > 0\}$ are invariant under the local flow. Moreover, all solutions starting in $\bar{\Omega} = \{(R, C, T) : R \geq 0, C \geq 0, T \geq 0\}$ are bounded forward in time and hence are defined for $[0, \infty)$.*

Proof The right-hand side of the system (1)–(3) are rational functions of R_n, C and T and are continuously differentiable and locally Lipschitz continuous. Thus, by the Picard Lindelöf theorem (Coddington and Levinson 1955 Theorem 3.1), these initial value problems have local unique solutions. Clearly, if $R_n = 0$, then $\dot{R}_n = 0$, and so on. Thus solutions starting on the coordinate planes stay on the coordinate planes. Hence, by uniqueness, solutions cannot cross the coordinate planes and the positive open and closed octants Ω and $\bar{\Omega}$ are invariant. Note that because all parameters are non-negative and $\bar{\Omega}$ includes non-negative values, the conditions $R_{n0} \neq \frac{-B_1}{\delta_r}$ and $C_0 \neq \frac{-B_2}{\delta_c}$ hold. To show that solutions in $\bar{\Omega}$ stay bounded for all positive times, consider the following.

Let h, j, n, and q be defined as the following:

$$h := \max\{a_n, \nu_2(V_{\max} + p)\}$$
$$n := \min\left\{\frac{\mu_n}{B1}, \frac{\mu_c}{B2}\right\}$$
$$j := \min\{\beta, \gamma\}$$
$$q := \frac{\Gamma + n}{2\kappa}$$

Note that h, j, n, and q are all positive since the parameters in the respective definitions are positive. Let $W = R + C + (\frac{h}{j})T$. Then, $W \geq 0$, and we have the following equations:

$$\frac{dW}{dt} = \frac{dR}{dt} + \frac{dC}{dt} + \left(\frac{h}{j}\right)\frac{dT}{dt},$$

which turns into the following after substituting the equation definitions:

$$= RT a_n - \mu_n \left(\frac{R}{B_1 + \delta_r R} \right) + v_2 \left(\frac{V_{\max} (\delta_n R)^2}{K_{mg}^2 + (\delta_n R)^2} + p \right) CT - \mu_c \left(\frac{C}{B_2 + \delta_c C} \right)$$
$$+ \left(\frac{h}{j} \right) T (\Gamma - \kappa T - \beta R - \gamma C).$$

Then, expanding and rearranging the terms, we get:

$$\leq a_n RT + \left(v_2 \frac{V_{\max} (\delta_n R)^2}{K_{mg}^2 + (\delta_n R)^2} + v_2 p \right) CT - \mu_n \left(\frac{R}{B_1 + \delta_r R} \right) - \mu_c \left(\frac{C}{B_2 + \delta_c C} \right)$$
$$- \beta \left(\frac{h}{j} \right) RT - \gamma \left(\frac{h}{j} \right) CT + \left(\frac{h}{j} \right) T (\Gamma - \kappa T).$$

Note that

$$\frac{V_{\max} (\delta_n R)^2}{K_{mg}^2 + (\delta_n R)^2} \leq V_{\max}, \quad \frac{R}{B_1 + \delta_r R} \leq \frac{1}{B_1} R, \text{ and } \frac{C}{B_2 + \delta_c C} \leq \frac{1}{B_2} C. \quad (39)$$

Then, we have the following inequality:

$$\frac{dW}{dt} \leq a_n RT + v_2 (V_{\max} + p) CT - \mu_n \left(\frac{1}{B_1} \right) R - \mu_c \left(\frac{1}{B_2} \right) C$$
$$- \beta \left(\frac{h}{j} \right) RT - \gamma \left(\frac{h}{j} \right) CT + \left(\frac{h}{j} \right) T (\Gamma - \kappa T).$$

Then, substituting h, n, j and q as defined previously, we get the following:

$$\frac{dW}{dt} \leq hRT + hCT - nR - nC - j \left(\frac{h}{j} \right) RT - j \left(\frac{h}{j} \right) CT + \left(\frac{h}{j} \right) T (\Gamma - \kappa T)$$

Which reduces to:

$$\frac{dW}{dt} = -n(R + C) + \left(\frac{h}{j} \right) T (\Gamma - \kappa T)$$

Finally, substituting back $W = R + C + (\frac{h}{j}) T$, this turns into:

$$\frac{dW}{dt} = -n(W - \left(\frac{h}{j} \right) T) + \left(\frac{h}{j} \right) T (\Gamma - \kappa T)$$
$$= -nW + \left(\frac{h}{j} \right) T + \left(\frac{h}{j} \right) T (\Gamma - \kappa T)$$
$$\leq -nW + q. \quad (40)$$

Then, $\frac{dW}{dt} \leq -nW + q$, and we get

$$W(t) \leq \frac{q}{n} + \left(W(0) - \frac{q}{n}\right)e^{-nt}. \tag{41}$$

Therefore, W is bounded along solutions for positive times starting in $\bar{\Omega}$. Thus, R_n, C and T are also bounded on $\bar{\Omega}$ for positive times. Since Ω is invariant, and solutions starting in $\bar{\Omega}$ stay bounded for positive times, the solutions exist for all positive times. □

As a direct consequence of (40) we have the following corollary which we will use when arguing the existence of optimal controls.

Corollary 1 *Using the notation and parameters as in Theorem* 6, *the compact* simplex

$$S' = \left\{(R, C, T) \in [0, \infty]^3 : W = R + C + \left(\frac{h}{j}\right)T \leq \frac{q}{n} + 1\right\} \tag{42}$$

is positively forward invariant under the flow of the system (1)–(3).

Proof From equation (40) it immediately follows that if $W > \frac{q}{n}$ then $\frac{dW}{dt} < 0$. □

Remark 1 The statements of Theorem 6 and Corollary 1 remain true if the system (1)–(3) is replaced by the system (4)–(6), or by system (11)–(13). Indeed, in the proof of Theorem 6 above, the second and third estimates in the inequalities (39) remain valid upon replacing $\delta_r R \geq 0$ and $\delta_c C \geq 0$ by $\sigma_1 u \geq 0$ and $\sigma_2 u \geq 0$, respectively.

References

Aït-Ali N, Fridlich R, Millet-Puel G, Clérin E, Delalande F, Jaillard C, Blond F, Perrocheau L, Reichman S, Byrne LC et al (2015) Rod-derived cone viability factor promotes cone survival by stimulating aerobic glycolysis. Cell 161(4):817–832

Aparicio A, Camacho ET, Philp NJ, Wirkus SA (2022) A mathematical model of GLUT1 modulation in rods and RPE and its differential impact in cell metabolism. Sci Rep 12(1):10645

Athans M, Falb PL (2013) Optimal control: an introduction to the theory and its applications. Courier Corporation

Besharse J, Bok D (2011) The retina and its disorders. Academic Press

Brennan LA, Lee W, Kantorow M (2010) Txnl6 is a novel oxidative stress-induced reducing system for methionine sulfoxide reductase a repair of α-crystallin and cytochrome c in the eye lens. PLoS ONE 5(11):e15421

Bryson AE (1975) Applied optimal control: optimization, estimation and control. CRC Press

Byrne LC, Dalkara D, Luna G, Fisher SK, Clérin E, Sahel J-A, Léveillard T, Flannery JG et al (2015) Viral-mediated RdCVF and RdCVFL expression protects cone and rod photoreceptors in retinal degeneration. J Clin Investig 125(1):105–116

Camacho ET, Dobreva A, Larripa K, Rădulescu A, Schmidt D, Trejo I (2021) Mathematical modeling of retinal degeneration: aerobic glycolysis in a single cone. From cells to populations, using mathematics to understand biological complexity, pp 135–178

Camacho ET, Wirkus S (2013) Tracing the progression of retinitis pigmentosa via photoreceptor interactions. J Theor Biol 317:105–118

Camacho E, Melara L, Villalobos M, Wirkus S (2014) Optimal control in the treatment of retinitis pigmentosa. Bull Math Biol 76:292–313

Camacho ET, Léveillard T, Sahel J-A, Wirkus S (2016) Mathematical model of the role of RdCVF in the coexistence of rods and cones in a healthy eye. Bull Math Biol 78(7):1394–1409

Camacho ET, Punzo C, Wirkus SA (2016) Quantifying the metabolic contribution to photoreceptor death in retinitis pigmentosa via a mathematical model. J Theor Biol 408:75–87

Camacho ET, Brager D, Elachouri G, Korneyeva T, Millet-Puel G, Sahel J-A, Léveillard T (2019) A mathematical analysis of aerobic glycolysis triggered by glucose uptake in cones. Sci Rep 9(1):4162

Camacho ET, Lenhart S, Melara LA, Villalobos MC, Wirkus S (2020) Optimal control with MANF treatment of photoreceptor degeneration. Math Med Biol A J IMA 37(1):1–21

Carruthers A (2016) GLUT1 structure, function and trafficking-regulation by cellular redox and metabolic status metabolic and redox signalling in the retina and central nervous system. http://www.college-de-france.fr/site/en-jose-alain-sahel/studyday-2016-03-16-14h45.htm

Chalmel F, Léveillard T, Jaillard C, Lardenois A, Berdugo N, Morel E, Koehl P, Lambrou G, Holmgren A, Sahel JA et al (2007) Rod-derived cone viability factor-2 is a novel bifunctional-thioredoxin-like protein with therapeutic potential. BMC Mol Biol 8(1):1–12

Clérin E, Wicker N, Mohand-Saïd S, Poch O, Sahel J-A, Léveillard T (2011) e-conome: an automated tissue counting platform of cone photoreceptors for rodent models of retinitis pigmentosa. BMC Ophthalmol 11(1):38

Coddington EA, Levinson N (1955) Theory of ordinary differential equations. Tata McGraw-Hill Education

Dobreva A, Camacho ET, Larripa K, Rădulescu A, Schmidt DR, Trejo I (2022) Insights into pathological mechanisms and interventions revealed by analyzing a mathematical model for cone metabolism. Biosci Rep 42(3):BSR20212457

Dobreva A, Camacho ET, Miranda M (2023) Mathematical model for glutathione dynamics in the retina. Sci Rep 13(1):10996

Elachouri G, Lee-Rivera I, Clérin E, Argentini M, Fridlich R, Blond F, Ferracane V, Yang Y, Raffelsberger W, Wan J et al (2015) Thioredoxin rod-derived cone viability factor protects against photooxidative retinal damage. Free Radic Biol Med 81:22–29

Filippov A (1962) On certain questions in the theory of optimal control. J Soc Ind Appl Math Ser A Control 1(1):76–84

Fleming WH, Rishel RW (1975) Deterministic and stochastic optimal control, vol 1. Springer, Berlin

Funato Y, Miki H (2007) Nucleoredoxin, a novel thioredoxin family member involved in cell growth and differentiation. Antioxid Redox Signal 9(8):1035–1058

Kanan Y, Hackett SF, Taneja K, Khan M, Campochiaro PA (2022) Oxidative stress-induced alterations in retinal glucose metabolism in retinitis pigmentosa. Free Radic Biol Med 181:143–153

Kirk DE (2004) Optimal control theory: an introduction. Courier Corporation

Lenhart S, Workman JT (2007) Optimal control applied to biological models. CRC Press

Léveillard T, Sahel J-A (2010) Rod-derived cone viability factor for treating blinding diseases: from clinic to redox signaling. Sci Transl Med 2(26):26ps16

Léveillard T, Sahel J-A (2017) Metabolic and redox signaling in the retina. Cell Mol Life Sci 74:3649–3665

Léveillard T, Mohand-Saïd S, Lorentz O, Hicks D, Fintz A-C, Clérin E, Simonutti M, Forster V, Cavusoglu N, Chalmel F et al (2004) Identification and characterization of rod-derived cone viability factor. Nat Genet 36(7):755–759

Léveillard T, Aït-Ali N et al (2017) Cell signaling with extracellular thioredoxin and thioredoxin-like proteins: insight into their mechanisms of action. Oxid Med Cell Longev 2017

Martin KR, Klein RL, Quigley HA (2002) Gene delivery to the eye using adeno-associated viral vectors. Methods 28(2):267–275

Matsuo I, Kimura-Yoshida C (2013) Extracellular modulation of fibroblast growth factor signaling through heparan sulfate proteoglycans in mammalian development. Curr Opin Genet Dev 23(4):399–407

McAsey M, Mou L, Han W (2012) Convergence of the forward-backward sweep method in optimal control. Comput Optim Appl 53(1):207–226

Mei X, Chaffiol A, Kole C, Yang Y, Millet-Puel G, Clérin E, Aït-Ali N, Bennett J, Dalkara D, Sahel J-A et al (2016) The thioredoxin encoded by the rod-derived cone viability factor gene protects cone photoreceptors against oxidative stress. Antioxid Redox Signal 24(16):909–923

Neustadt LW (1963) The existence of optimal controls in the absence of convexity conditions. J Math Anal Appl 7(1):110–117

Petit L, Ma S, Cipi J, Cheng S-Y, Zieger M, Hay N, Punzo C (2018) Aerobic glycolysis is essential for normal rod function and controls secondary cone death in retinitis pigmentosa. Cell Rep 23(9):2629–2642

Phillips MJ, Otteson DC, Sherry DM (2010) Progression of neuronal and synaptic remodeling in the rd10 mouse model of retinitis pigmentosa. J Comp Neurol 518(11):2071–2089

Pontryagin LS (1987) Mathematical theory of optimal processes. CRC Press

Royden HL, Fitzpatrick P (1988) Real analysis, vol 32. Macmillan, New York

Shintani K, Shechtman DL, Gurwood AS (2009) Review and update: current treatment trends for patients with retinitis pigmentosa. Optom J Am Optometr Assoc 80(7):384–401

Steinmetz JD, Bourne RR, Briant PS, Flaxman SR, Taylor HR, Jonas JB, Abdoli AA, Abrha WA, Abualhasan A, Abu-Gharbieh EG et al (2021) Causes of blindness and vision impairment in 2020 and trends over 30 years, and prevalence of avoidable blindness in relation to vision 2020: the right to sight: an analysis for the global burden of disease study. Lancet Glob Health 9(2):e144–e160

Wifvat K, Camacho ET, Wirkus S, Léveillard T (2021) The role of RdCVFL in a mathematical model of photoreceptor interactions. J Theor Biol 520:110642